The Plant Cell, Vol. 22: 1388–1403, April 2010, www.plantcell.org © 2010 American Society of Plant Biologists

Translocation of *Magnaporthe oryzae* Effectors into Rice Cells and Their Subsequent Cell-to-Cell Movement [W] [OA]

Chang Hyun Khang,[a,1] Romain Berruyer,[a,1,2] Martha C. Giraldo,[a] Prasanna Kankanala,[a,3] Sook-Young Park,[b,4] Kirk Czymmek,[c] Seogchan Kang,[b] and Barbara Valent[a,5]

[a] Department of Plant Pathology, Kansas State University, Manhattan, Kansas 66506
[b] Department of Plant Pathology, Pennsylvania State University, University Park, Pennsylvania 16802
[c] Department of Biological Sciences and Delaware Biotechnology Institute, University of Delaware, Newark, Delaware 19711

Knowledge remains limited about how fungal pathogens that colonize living plant cells translocate effector proteins inside host cells to regulate cellular processes and neutralize defense responses. To cause the globally important rice blast disease, specialized invasive hyphae (IH) invade successive living rice (*Oryza sativa*) cells while enclosed in host-derived extrainvasive hyphal membrane. Using live-cell imaging, we identified a highly localized structure, the biotrophic interfacial complex (BIC), which accumulates fluorescently labeled effectors secreted by IH. In each newly entered rice cell, effectors were first secreted into BICs at the tips of the initially filamentous hyphae in the cell. These tip BICs were left behind beside the first-differentiated bulbous IH cells as the fungus continued to colonize the host cell. Fluorescence recovery after photobleaching experiments showed that the effector protein PWL2 (for prevents pathogenicity toward weeping lovegrass [*Eragrostis curvula*]) continued to accumulate in BICs after IH were growing elsewhere. PWL2 and BAS1 (for biotrophy-associated secreted protein 1), BIC-localized secreted proteins, were translocated into the rice cytoplasm. By contrast, BAS4, which uniformly outlines the IH, was not translocated into the host cytoplasm. Fluorescent PWL2 and BAS1 proteins that reached the rice cytoplasm moved into uninvaded neighbors, presumably preparing host cells before invasion. We report robust assays for elucidating the molecular mechanisms that underpin effector secretion into BICs, translocation to the rice cytoplasm, and cell-to-cell movement in rice.

INTRODUCTION

Intracellular animal and plant pathogens, including the rice blast fungus, spend at least the early stages in living host cells sequestered from the host cytoplasm by a membrane (O'Connell and Panstruga, 2006; Bhavsar et al., 2007; Kankanala et al., 2007). To achieve biotrophic colonization, these pathogens deliver a subset of effector proteins, termed cytoplasmic effectors, into host cells to dampen defenses and assume control (Bhattacharjee et al., 2006; Ellis et al., 2006; Bhavsar et al., 2007; Kamoun, 2007; Whisson et al., 2007). For the eukaryotic pathogens, which are less-studied than prokaryotic pathogens, this raises the major question of how effectors are delivered across the plasma membrane to reach the host cytoplasm. We are addressing this question by studying rice blast disease, which is caused by the hemibiotrophic, ascomycetous fungus *Magnaporthe oryzae* (Couch et al., 2005; Dean et al., 2005; Ebbole, 2007; Wilson and Talbot, 2009). Rice blast continues to pose a threat to global food supplies despite decades of effort to control this disease (Wang and Valent, 2009). For rice blast, effectors are predicted to be delivered into the host cytoplasm to promote the susceptible (compatible) interaction, but evidence supporting such a role is currently lacking. Several putative cytoplasmic effectors have been identified as avirulence (*AVR*) gene products whose recognition by rice resistance (*R*) gene products triggers the hypersensitive response (HR) and resistance (incompatible interaction). Over 80 such blast *R* genes have been identified so far in the search for durable resistance to rice blast disease (Ballini et al., 2008), suggesting that many *AVR* effector genes remain to be identified.

Hemibiotrophy in blast disease is characterized by successive biotrophic invasions of rice (*Oryza sativa*) cells by intracellular invasive hyphae (IH) that are surrounded by a plant-derived extrainvasive hyphal membrane (EIHM) (Kankanala et al., 2007). For each new cell entry, the fungus initially grows as a thin filamentous hypha, the primary hypha in the first-invaded cell or filamentous IH in subsequently invaded cells (Heath et al., 1990; Kankanala et al., 2007). In compatible interactions, these filamentous hyphae differentiate into bulbous IH, and invaded plant cells retain intact plasma membranes and the ability to plasmolyze (Koga et al., 2004; Kankanala et al., 2007). With plasmolysis, the host plasma membrane does not separate from the IH. Instead, IH are always surrounded by the shrunken plant

[1] These authors contributed equally to this work.
[2] Current Address: Université d'Angers, 49045 Angers, France.
[3] Current Address: Edenspace Systems Corporation, Manhattan, KS 66502.
[4] Current Address: Center for Fungal Pathogenesis, Seoul National University, Seoul, Korea.
[5] Address correspondence to bvalent@ksu.edu.
The author responsible for distribution of materials integral to the findings presented in this article in accordance with the policy described in the Instructions for Authors (www.plantcell.org) is: Barbara Valent (bvalent@ksu.edu).
[W] Online version contains Web-only data.
[OA] Open Access articles can be viewed online without a subscription.
www.plantcell.org/cgi/doi/10.1105/tpc.109.069666

protoplast (Kankanala et al., 2007). Thus, intracellular invasion by the blast fungus differs from the invasion by rust and mildew fungi, which grow extracellularly and produce intracellular haustoria separated from host cytoplasm by extrahaustorial membrane (Mendgen and Hahn, 2002; O'Connell and Panstruga, 2006).

Determining the nature of the interface between blast IH and the host cytoplasm is critical for understanding translocation of blast effectors into the host cytoplasm. So far, two lines of evidence suggest that IH are sealed within a distinct apoplastic compartment that is separated from both the symplast and the bulk apoplast. First, the endocytotic tracker dye FM4-64 stains the EIHM and other plant membranes, but it is excluded from IH membranes in fully compatible infection sites (Kankanala et al., 2007). This would occur if the EIHM forms a sealed compartment that prevents dye from reaching the IH membranes. Second, fluorescently labeled BAS4, a putative EIHM matrix protein, precisely outlines IH without observable diffusion into the apoplast (Mosquera et al., 2009). In some compatible infection sites, generally characterized by nonuniform BAS4 outlining of IH, BAS4 appeared to have spilled into the host cell cytoplasm. Therefore, the EIHM compartment containing blast IH appears analogous to extrahaustorial compartments of rusts that are separated from the host apoplast by a neckband (Mendgen and Hahn, 2002; O'Connell and Panstruga, 2006) or to the parasitophorous vacuole that completely encloses the malarial pathogen, *Plasmodium falciparum*, inside invaded red blood cells (Bhattacharjee et al., 2006, 2008).

Growing evidence suggests that proteins secreted by IH play a major role in the early postpenetration stages of blast disease when the fungus succeeds in biotrophic invasion or is recognized and defeated by the plant. Recently, Yi et al. (2009) have shown that *M. oryzae* mutants lacking the lumenal heat shock protein seventy (*LHS1*) gene, which encodes an endoplasmic reticulum (ER) chaperone functioning in protein secretion, were severely impaired in biotrophic invasion and in induction of *R* gene–mediated HR. These same mutants showed minor impairment of axenic growth in nutrient medium. Additionally, fungal genes that are upregulated during biotrophic invasion are highly enriched for genes encoding biotrophy-associated secreted (BAS) proteins (Mosquera et al., 2009). Except for the Avirulence Conferring Enzyme1 gene (Böhnert et al., 2004), all known blast *AVR* genes encode small BAS proteins. These include *PWL1* from finger millet (*Eleusine coracana*) isolates and *PWL2* from rice isolates, which both function at the host species level by preventing strains that contain them from infecting weeping lovegrass, *Eragrostis curvula* (Kang et al., 1995; Sweigard et al., 1995). *AVR-Pita1* (Orbach et al., 2000; Khang et al., 2008), which confers AVR toward rice containing the corresponding *R* gene *Pita* (Bryan et al., 2000), encodes a putative zinc metalloprotease. Additional cloned *AVR* genes are *AVR1-CO39* and *AvrPiz-t*, which were identified by map-based cloning (Farman and Leong, 1998; Li et al., 2009), *AVR-Pii* and *AVR-Pik/km/kp*, which were identified by fungal genome resequencing and association genetics (Yoshida et al., 2009), and *AVR-Pia*, which was cloned independently using association genetics and spontaneous mutant analysis (Shinsuke et al., 2009; Yoshida et al., 2009). Transient expression of AVR-Pita1, AVR-Pia, AVR-Pii, and AVR-Pik/km/kp proteins in rice with the cognate *R* gene product suggested that they function after secretion from the fungus and translocation into the rice cytoplasm (Jia et al., 2000; Yoshida et al., 2009).

As a step toward understanding the mechanism of effector secretion and translocation in rice blast disease, we observed IH growing in rice cells and secreting AVR effectors fused with a fluorescent protein. These proteins accumulated in a novel structure, the biotrophic interfacial complex (BIC). BIC development is coupled to hyphal differentiation from filamentous to pseudohyphal (Veses and Gow, 2009) bulbous IH growth, which is required for disease development. PWL2 and BAS1, pathogen-secreted proteins that are preferentially localized to BICs, were also translocated to the rice cytoplasm, but BAS4, a more generally distributed putative EIHM matrix protein, was not. Fluorescent proteins that reached the invaded cell's cytoplasm moved into adjoining uninvaded rice cells in a manner that is dependent on protein size and rice cell type, consistent with transport through plasmodesmata. This research reveals important details about biotrophic invasion in rice blast disease and provides robust assays for molecular analyses of effector secretion, translocation, and cell-to-cell movement.

RESULTS

Two-Stage Development of BICs in Successively Invaded Rice Cells

In initial efforts to understand effector secretion and translocation in planta, we produced fungal transformants that express translational fusions with enhanced green fluorescent protein (EGFP) or variants of monomeric red fluorescent protein (mRFP) at the C termini of various portions of the blast effectors AVR-Pita1, PWL1, and PWL2 (see Supplemental Figure 1 and Supplemental Table 1 online). Unless indicated otherwise, all effector:fluorescent protein (FP) constructs were under control of the native promoters. Individual constructs were introduced into *M. oryzae*, and resulting transformants were analyzed for fluorescent protein secretion in rice sheath epidermal cells. For all three effectors, fusion proteins containing the entire effector coding sequence and EGFP conferred the expected host specificity. Fungal transformants containing AVR-Pita1:EGFP fusions induced resistance in rice carrying the *R* gene *Pita* (see Supplemental Figures 2A to 2H online). Fungal transformants expressing PWL1:EGFP or PWL2:EGFP no longer infected weeping lovegrass (see Supplemental Figures 2I and 2J online), even when they were derived from the highly aggressive weeping lovegrass pathogen 4091-5-8 (Sweigard et al., 1995).

Without a signal peptide in the construct, the *AVR-Pita1*, *PWL1*, and *PWL2* promoters produced uniform cytoplasmic EGFP fluorescence in IH (Figure 1A; see Supplemental Figure 3A online). By contrast, the fluorescently labeled AVR-Pita1 and PWL effectors showed secretion and localized accumulation in a novel structure, which we named the BIC (Figure 1B, left panels; see Supplemental Figures 3A to 3G online). Using effector promoters and EGFP, we demonstrated that each of the effector signal peptide sequences and the AVR-Pita preprosequence

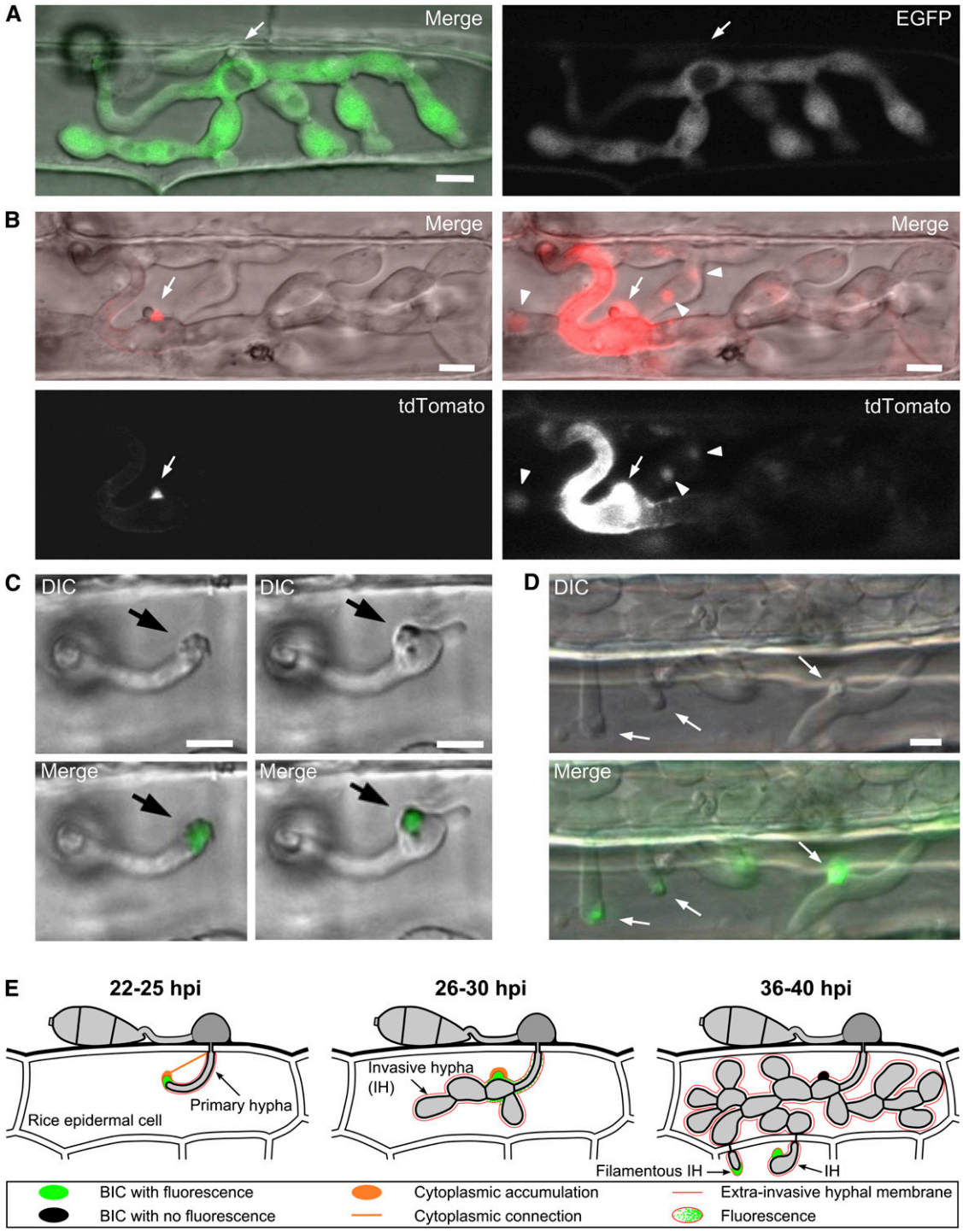

Figure 1. Two-Stage BIC Development and Preferential Effector Accumulation in Successively Invaded Rice Sheath Cells.

For all images, arrows indicate BICs. Bars = 5 μm.

(A) Fungal cytoplasmic EGFP (showing exclusion from the vacuoles) after expression by transformant P1-1-3 using the *PWL1* promoter (30 HAI). Shown are confocal images of merged bright-field and fluorescence (left) and fluorescence alone as white (right; the arrow indicates the position of the BIC, which is not fluorescent here).

(B) Restricted accumulation of PWL2:tdTomato (red) in a BIC (arrow) and around BIC-associated cells as transformant KV106 invades a YT16 rice cell at 27 HAI. Left: Confocal image with an optimal pinhole (one airy unit) shows the BIC accumulation of PWL2:tdTomato (red). Note the BIC-associated dark round body that is adjacent to the BIC on the left. Right: Confocal image with an open pinhole (10.07 airy units, almost a nonconfocal image) showed

also mediated accumulation in BICs (Figures 1C and 1D; see Supplemental Figures 3A and 3G online). The following pattern of BIC development is based on observation of >2000 independent infection sites. Immediately after appressorial penetration (Figures 1C and 1D; see Supplemental Figures 3B and 3G online), filamentous primary hyphae secreted effector:FP into membrane caps, which are the membrane-rich extensions of the EIHM at the primary hyphal tips (Kankanala et al., 2007). When primary hyphae had differentiated into bulbous IH, fluorescence was observed in a small body adjacent to the first-formed IH cell (Figure 1B; see Supplemental Figure 3C online). Time-lapse imaging demonstrated that the hyphal tip BIC is left behind when the hypha switches to pseudohyphal growth, becoming the structure apposed to the first IH cell (Figure 1C; see Supplemental Movie 1 online). Accumulation of fluorescent effector proteins in BICs appeared to be a feature of the compatible biotrophic interaction because effector-labeled BICs were not observed in the AVR-Pita1–mediated incompatible interaction (Mosquera et al., 2009) or when IH-like hyphae formed in vitro (see Supplemental Figure 4 online).

Primary fluorescent BICs inside first-invaded rice cells remained at the same location beside the first differentiated IH cell as long as the fungus continued to grow in that rice cell, even until later stages when IH had completely filled the cell (Figure 1B; see Supplemental Figure 3D online). Primary BICs can be recognized even without fluorescence due to their significant size (>1 μm diameter) in first-invaded cells and their predictable location, typically determined by following the curve of the primary hypha to a position beside the first IH cell. Additionally, a nonfluorescent, phase-contrast dark round body was often observed near the primary BIC (Figure 1B), and the IH cell adjacent to the BIC often contained a relatively large vacuole (Figure 1A). To quantify primary BIC formation, we examined 1235 individual infection sites (n = 535 for Ft080; n = 700 for Ft102) for the presence of a BIC and occurrence of EGFP fluorescence. Primary BICs were visible at >98% of the infection sites, and fluorescence was detectable in ~88% of the BICs. To investigate the generality of BIC formation, we determined that fluorescent BICs were formed when IH invaded barley epidermal cells (see Supplemental Figure 3H online) and that eight additional rice isolates collected worldwide also formed BICs (see Supplemental Table 1 and Supplemental Figure 3I online).

After completely filling first-invaded epidermal cells, IH undergo extreme constriction to cross the plant cell wall and then initially grow as filamentous IH resembling primary hyphae in the first cells (Kankanala et al., 2007). When IH moved into neighboring cells, fluorescence generally disappeared in the first-invaded cells. In newly invaded cells, fluorescence was detected in membrane caps at the tips of the filamentous IH (Figure 1D; see Supplemental Figure 3E online). Again, the fluorescent membrane caps became BIC bodies adjacent to IH cells (Figure 1D; see Supplemental Figure 3F online). Secondary BICs in subsequently invaded cells were smaller than primary BICs and were only reliably identified by fluorescence. Fluorescent secondary BICs were identified on ~85% of hyphae at 793 infection sites. BIC fluorescence disappeared when the fungus exited a cell and was reestablished in BICs in newly invaded cells. The two stages of BIC development were precisely correlated with differentiation of the biotrophic filamentous hypha into bulbous IH for each hypha in successively invaded rice cells (Figure 1E).

We observed dynamic cytoplasmic accumulations around BICs at early stages of host cell invasion, and the BIC regions were often interconnected with cytoplasm that accumulated beneath the appressorial penetration site (Figures 2A to 2D). For example, live-cell imaging documented host cytoplasmic strands connecting the membrane cap regions of primary hyphae to the appressorial penetration sites (Figure 2A; see Supplemental Movie 2 online). In another example, live-cell imaging documented a fluorescent BIC surrounded by dynamically shifting rice cytoplasm after moving beside the IH cell (Figures 2B to 2D). A cytoplasmic connection emanating from the BIC region toward the appressorial penetration site appeared (Figure 2C) and then was no longer visible (Figure 2D). Such cytoplasmic dynamics are characteristic of healthy plant cells (Verma and Hong, 2005), suggesting that minimal damage has occurred to the invaded host cell.

Effector:FPs Preferentially Accumulate in BICs

Although effector:FPs accumulated to the highest levels in BICs, conventional epifluorescence images with longer exposure times showed significant fluorescence outlining the hyphal cells associated with the BIC (the primary hypha and the first IH cell) and little fluorescence around subsequent IH cells. This can also be observed by increasing the pinhole diameter to allow more collection of fainter signals during confocal microscopy. For example, confocal imaging of a BIC with standard pinhole and optimal detector settings (1 airy unit) showed BIC accumulation of PWL2 fused to tandem dimer (td) Tomato (Shaner et al., 2008), which is a genetic fusion of two copies of an mRFP variant with brighter fluorescence (Figure 1B, left). Increasing the pinhole diameter (to 10 airy units) allowed detection of weaker PWL2:

Figure 1. (continued).

fluorescence concentrated around BIC-associated cells (primary hypha and first IH cell). PWL2:tdTomato accumulated in presumed vacuoles (arrowheads) in non-BIC IH cells, including one that branched from the primary hypha (on left). Top images: Merged bright-field and fluorescence. Bottom: Fluorescence as white.

(C) First (left) and last (right, 90 min later) frames of Supplemental Movie 1 online (wide-field microscopy) demonstrating that the BIC from the primary hyphal tip was left behind when this hypha switched to bulbous IH growth. This is strain Ft080 expressing EGFP with the *AVR-Pita1* promoter and signal peptide in a Yashiro-mochi cell. Merge shows DIC and EGFP images.

(D) BIC development was repeated by Ft080 hyphae (same as in **[C]**) entering neighbor cells at 40 HAI. Wide-field microscopy with merge showing DIC and EGFP images.

(E) Schematic diagram summarizing events involved in BIC development.

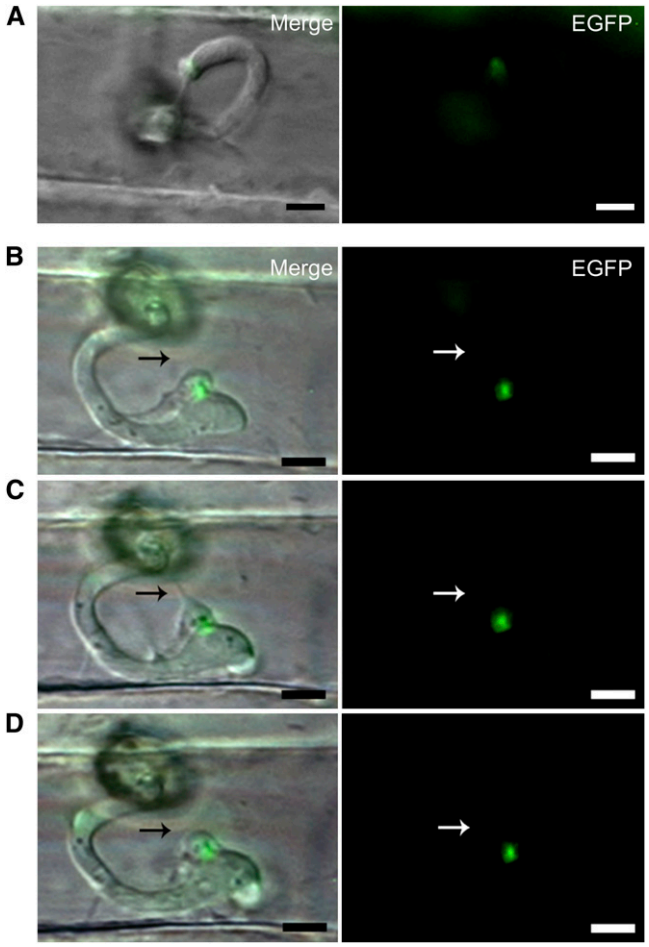

Figure 2. Transient Cytoplasmic Connections Tether the BIC Region to the Appressorial Penetration Site.

Conventional fluorescence microscopy was used. Merge shows DIC and fluorescence images (left) and fluorescence alone (right).
(A) A middle-frame image from Supplemental Movie 2 online in which a cytoplasmic strand connects a primary hyphal tip to the region of appressorial penetration. Faint BIC fluorescence is seen as transformant KV60 expressed and secreted EGFP with the P27 promoter and AVR-Pita1 signal peptide in YT16 rice at 27 HAI.
(B) to **(D)** Shifting cytoplasm around an EGFP-labeled BIC shown in time-lapse images (40- and 33-min intervals, respectively) of KV88 in YT16 rice, secreting EGFP as in **(A)**. A cytoplasmic connection (arrow) between the BIC region and appressorial penetration zone in **(C)** was not visible 33 min later in **(D)**. Bars = 5 μm.

tdTomato fluorescence that had accumulated around the BIC-associated cells (Figure 1B, right). Some weak red fluorescence occurred in vacuoles in non-BIC-associated IH cells, but little or no red fluorescence was observed outlining these IH cells (Figure 1B, right). Localization restricted to BICs and around BIC-associated cells is hereafter referred to as preferential BIC accumulation.

To test if preferential BIC accumulation is due to a continuous secretion of effector:FPs into BICs, we used the fluorescence recovery after photobleaching (FRAP) technique. We selectively photobleached PWL2:EGFP fluorescence in a primary hyphal tip BIC and then monitored fluorescence recovery over time. After near complete elimination, fluorescence fully recovered within 2.5 h (Figure 3). During this experiment, the tip BIC became a side BIC and new IH grew from the BIC-associated cells. Fluorescence was not visible around these subsequently growing IH cells during the BIC recovery period. This result was confirmed in two independent FRAP experiments. It appeared that fluorescent effector proteins continued to be synthesized and delivered to BICs while IH were actively growing elsewhere.

Effector Promoter and Signal Peptide-Encoding Sequences Confer Preferential BIC Accumulation

Using the native effector promoters, we found that the signal peptide-encoding sequences were interchangeable with entire protein coding sequences for targeting EGFP to BICs ($n > 1000$; Figures 1C and 1D; see Supplemental Figures 3A and 3G online).

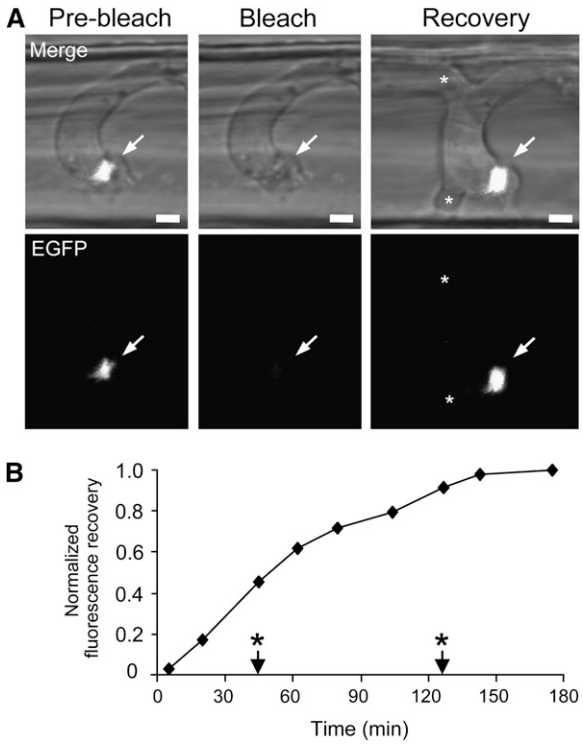

Figure 3. FRAP Demonstrates Continuous Secretion of PWL2:EGFP into the BIC.

(A) Confocal FRAP images of KV105 secreting PWL2:EGFP into a BIC in a YT16 cell. Fluorescence in a hyphal tip BIC (Pre-bleach) was photobleached at 27 HAI (Bleach) and allowed to recover for 175 min (Recovery). Asterisks mark new IH cells that grew during this period. Arrows indicate the BIC. EGFP fluorescence is shown in white. Merge shows bright-field and EGFP. Bars = 2 μm.
(B) Plot of normalized BIC fluorescence intensity recovery over time. Arrows with asterisks indicate when new hyphal branches emerged; top branch first observed at 45 min and bottom branch at 127 min.

Using the *BAS4* promoter, the *BAS4* signal peptide-encoding sequence was interchangeable with the entire protein coding sequence in mediating secretion of EGFP in the IH-outlining pattern ($n > 300$; see Supplemental Figure 5 online; Mosquera et al., 2009). To further test if preferential BIC accumulation is specific for effector promoter and signal peptide sequences, we expressed EGFP under control of the constitutive ribosomal protein P27 promoter and fused to the N-terminal 26 amino acids of Cutinase 1 (CUT1; MGG_01943.6). The CUT1 signal peptide (CUT1SP, N-terminal 16 amino acids) mediates secretion of a cutin-degrading enzyme with a likely role during the prepenetration or nectrotrophic stages; thus, it is unlikely to be a cytoplasmic effector protein (Sweigard et al., 1992). We determined secretion patterns for fungal transformants that expressed P27:CUT1SP:EGFP, together with a BIC localization control, PWL2:mRFP. In contrast with the preferential BIC accumulation pattern of PWL2:mRFP, the P27:CUT1SP:EGFP gene product ($n = 25$ infection sites) was secreted and localized similarly to BAS4:FP, with accumulation around the IH and minimal BIC accumulation (Figure 4). These results indicate that motifs or features responsible for preferential BIC accumulation reside somewhere within the promoter and/or signal peptide-encoding sequences.

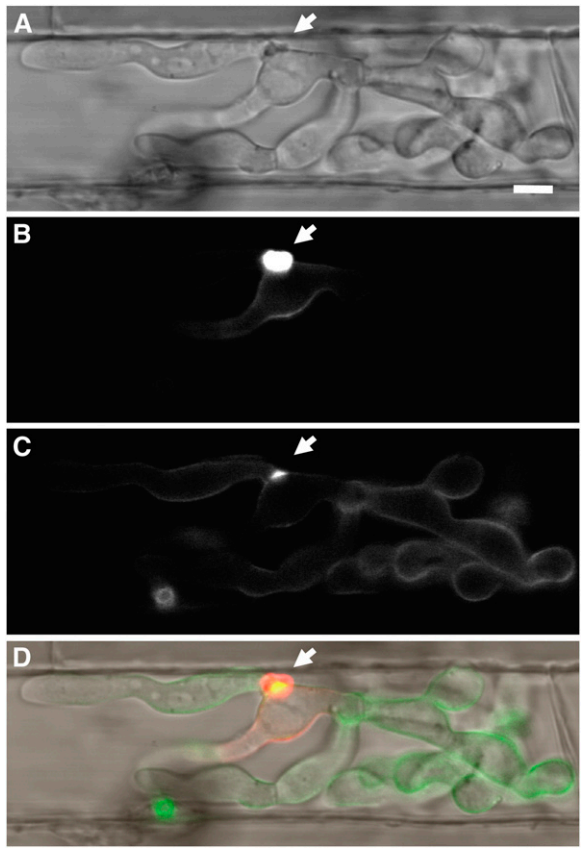

Figure 4. Noneffector Promoter and Signal Peptide Sequences Do Not Confer Preferential BIC Localization.

Confocal image of KV107 expressing EGFP with the P27 promoter and the Cutinase 1 signal peptide (P27:CUT1SP:EGFP) together with PWL2:mRFP in YT16 at 32 HAI. Arrow indicates BIC. Pinhole settings are 2 airy units for mRFP and 5 airy units for EGFP. Bar = 5 μm.

(A) Bright-field image.

(B) PWL2:mRFP fluorescence (red shown as white) showed preferential BIC accumulation.

(C) P27:CUT1SP:EGFP fluorescence (green shown as white) outlined IH with weak fluorescence in the BIC.

(D) Merged bright-field, mRFP (red), and EGFP (green) images. Yellow indicates overlapping mRFP and EGFP fluorescence.

Translocation of Fluorescent Effector Proteins to the Rice Cytoplasm

To demonstrate effector translocation, we focused on *PWL2*, which is expressed at higher levels than *AVR-Pita1* (Mosquera et al., 2009). The PWL2:FP transformants also expressed the putative matrix protein BAS4:FP (Mosquera et al., 2009). Using confocal microscopy with optimal pinhole conditions for observation of BICs, we generally did not observe fluorescence in the rice cytoplasm. However, PWL2-associated fluorescence was observed in invaded host cells after increasing the pinhole diameter (and, thus, optical slice thickness) and permitting the collection of relatively weak fluorescence signals (Figure 5A).

We also observed faint PWL2-associated fluorescence in the cytoplasm of invaded cells using conventional fluorescence microscopy and longer exposure times such that BIC fluorescence was saturated (Figures 5B to 5D). To concentrate the putative cytoplasmic fluorescence and move it away from the plant cell wall, we used a gentle stepwise plasmolysis procedure (Figures 5B to 5D) that minimizes host cell damage (Mellersh and Heath, 2001). Using PWL2 fused to tdTomato (Figure 5B), mRFP (Figure 5C), and EGFP (Figure 5D), the corresponding fluorescence was observed in the invaded host cell, and it precisely followed the pattern of plasmolyzed rice cytoplasm, namely, a thin layer of cytoplasm surrounding a large vacuole. Putative rice nuclei were also fluorescent. The PWL2:FP cytoplasmic fluorescence pattern was not observed in extensive autofluorescence controls ($n > 150$ images) that we routinely performed together with experimental observations (see Supplemental Figures 6A and 6B online).

Surprisingly, PWL2:mRFP fluorescence was frequently observed in the cytoplasm and nuclei of adjoining cells that did not contain IH (Figure 5C). Indeed, mRFP fluorescence could be observed two to four neighbor cells deep surrounding the invaded cell as early as 28 h after inoculation (HAI; see Supplemental Figure 6D online). We hypothesized that this could occur by movement of translocated PWL2:mRFP protein into adjoining host cells through plasmodesmata, the symplastic channels between rice cells, as has been reported for GFP in some plant tissues (Oparka et al., 1999; Zambryski, 2004).

Conventional epifluorescence microscopy allowed robust quantitation of PWL2:FP translocation using IH expressing PWL2:mRFP and BAS4:EGFP at ~27 HAI (Figures 5C and 6A), as well as IH expressing PWL2:EGFP and BAS4:mRFP as reversed reporter controls (Figures 5D and 6B). For all infection sites, fluorescence images were captured as a series with increasing exposure times to optimize visualization of strong BAS4 outlining of IH and faint translocation into rice cells at the fluorescence extremes (see Supplemental Figures 6F and 6G

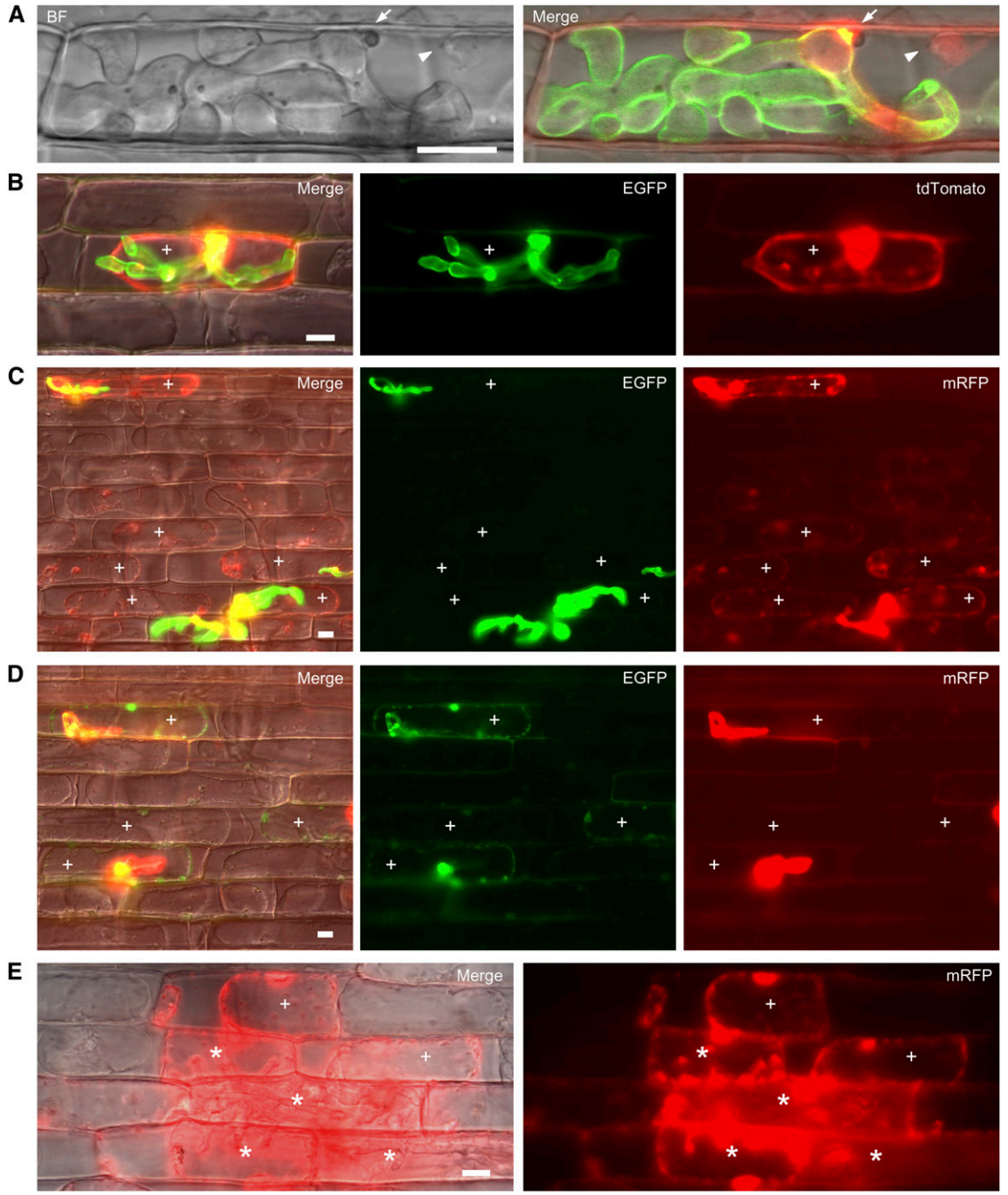

Figure 5. PWL2:FPs, but Not BAS4:FPs, Are Translocated into the Rice Cytoplasm.

Yellow (overlapping of green and red) in merged images indicates BIC-associated cells. Bars = 10 μm.

(A) Confocal image of KV104 showing preferential BIC localization of PWL2:mRFP (red) and presumed translocation into invaded YT16 cytoplasm at 31 HAI. BAS4:EGFP (green) was seen outlining the IH but not in the rice cytoplasm. Pinhole settings are 1 airy unit for EGFP and 5 airy units for mRFP. Arrow indicates BIC. Arrowhead indicates presumed nucleus. Merge shows bright-field (BF), EGFP, and mRFP images.

(B) to **(D)** Conventional epifluorescence microscopy after sucrose-induced plasmolysis. Plus signs indicate selected rice protoplasts that contain cytoplasmic fluorescence in the PWL2:FP channel. Merge shows DIC, EGFP, and mRFP (or tdTomato in **[B]**).

(B) PWL2:tdTomato (red), but not BAS4:EGFP (green), was translocated to the cytoplasm of a rice cell invaded by KV106 at 30 HAI. PWL2:tdTomato fluorescence was not observed in adjoining cells. Exposure times were 2 s for both EGFP and tdTomato.

(C) PWL2:mRFP (red), but not BAS4:EGFP (green), was translocated to the cytoplasm of rice cells invaded by KV104 at 27 HAI. mRFP fluorescence occurs in the cytoplasm of uninvaded neighbors around regular invaded epidermal cells (bottom right), but not around the invaded vein-associated cell

online). Considering PWL2:mRFP, all but one of the 286 (~100%) plasmolyzed invaded rice cells had mRFP fluorescence in their cytoplasm, and the mRFP was observed in adjoining cells at 260 (91%) of the sites with cytoplasmic fluorescence (Figures 5C and 6A, red ovals). Considering PWL2:EGFP, 149 (71%) of the 210 plasmolyzed invaded rice cells had EGFP fluorescence in their cytoplasm, and the EGFP was observed in uninvaded adjoining cells at 124 (83%) of the sites with cytoplasmic fluorescence (Figures 5D and 6B, green ovals). These results showed that PWL2:FP translocation was routinely observed when care was taken to visualize faint fluorescence and to differentiate this fluorescence from host autofluorescence. The movement of PWL2:FP into uninvaded neighbors supported our conclusion that PWL2:FP had reached the cytoplasm of living rice cells.

In contrast with results with PWL2:FPs, BAS4:FPs were rarely observed in the rice cytoplasm (Figure 6A, green ovals; Figure 6B, red ovals). As predicted by Mosquera et al. (2009), most infection sites with BAS4:FPs in the host cytoplasm were sites with discontinuous BAS4:FP outlining and likely EIHM breakage and spillage of matrix proteins (see Supplemental Figure 6E online). Interestingly, BAS4:FPs were more often observed in the rice apoplast, as visualized in the extracellular space between the rice cell wall and shrunken protoplast. At infection sites with IH secreting BAS4:EGFP, 11% showed green fluorescence in the apoplast, but not in the cytoplasm (green-shaded rectangles with black ovals in Figure 6A; see Supplemental Figure 6F online). At infection sites with IH secreting BAS4:mRFP, 52% showed red fluorescence in the apoplast, but not in the cytoplasm (red-shaded rectangles with black ovals in Figure 6B; see Supplemental Figure 6G online). Most of these infection sites had PWL2:FP in the rice cytoplasm. By contrast, apoplastic localization of PWL2:FP fusion proteins was only observed in two sites (<1%) with PWL2:mRFP and not at all in sites with PWL2:EGFP. Host apoplastic localization, and not cytoplasmic localization, appears to be a characteristic of BAS4:FPs.

We tested BAS1, a biotrophy-associated secreted protein showing preferential BIC accumulation (Mosquera et al., 2009), for rice translocation. Like PWL2 and unlike BAS4, BAS1 was observed to have translocated into the cytoplasm of invaded rice cells (n = 25). BAS1 had also moved ahead into uninvaded neighbors (Figure 5E). So far, preferential BIC accumulation is correlated with translocation of effectors into the rice cytoplasm.

Nuclear Targeting of Fluorescent Effectors Facilitates Visualization of Translocation and Cell-to-Cell Spread

To more easily visualize faint fluorescence from translocation of PWL2:FPs in nonplasmolyzed rice cells, we used two strategies to target PWL2 with C-terminal mCherry, an improved version of mRFP, to the host nucleus (Figure 7). First, we added a small nuclear localization signal (NLS) from simian virus large T-antigen (Ai et al., 2007) at the C terminus of the PWL2:mCherry fusion (PWL2:mCherry:NLS, 44.5 kD); second, we added histone H1 (hH1) from *Neurospora crassa* as a nuclear targeting sequence between PWL2 and mCherry (PWL2:hH1:mCherry, 66.1 kD). At successful infection sites with uniform BAS4 outlining, PWL2:mCherry:NLS (n = 41) and PWL2:hH1:mCherry (n = 103) exhibited significant fluorescence in BICs and in nuclei of invaded host cells (Figures 7A, 7B, and 7D). Indeed, fluorescence could be observed in rice nuclei at an early stage of infection, when primary hyphae were still growing in the host cell (Figure 7A). Fluorescence intensity was high in the nucleus of invaded cells, and reduced intensity was often observed in nuclei of surrounding cells (Figure 7B). By contrast, when we expressed the mCherry:NLS protein at the C terminus of BAS4 (BAS4:mCherry:NLS) along with BAS4:EGFP, both green and red fluorescence were observed in the IH-outlining pattern. BAS4 fluorescence was not observed inside the rice cells (Figure 7C). The results with nuclear targeting of fluorescent effector proteins were consistent with results from the plasmolysis assay (Figure 6). This nuclear targeting assay provides sensitive detection of effector translocation into host cells and of cell-to-cell trafficking after translocation.

Cell-to-Cell Movement Is Dependent on Rice Cell Type and Effector:FP Size

We noticed that when the long and narrow epidermal cells overlying the sheath vascular tissue were invaded, they showed especially bright fluorescence from the translocated PWL2 fusion proteins, with only rare examples of movement of the fluorescent proteins to neighbor cells (Figures 5C and 7A). Indeed, 23 invaded vein-associated cells were included in the quantitative analysis (Figure 6A), and these comprised 23 of the 25 examples in which mRFP fluorescence was restricted to the invaded cell. PWL2:mRFP fluorescence was presumably brighter in vein-associated cells because it accumulated there instead of spreading to adjoining cells. To confirm this, we quantitated cell-to-cell movement in vein-associated and regular epidermal cells with the nuclear-targeted PWL2:mCherry:NLS and PWL2:hH1:mCherry constructs (Table 1). For both constructs, fluorescence was restricted to the invaded vein-associated cell at 92% of the infection sites. In the 8% of sites with cell-to-cell movement, only faint fluorescence was detected in the most immediate neighbors. In the same experiments, cell-to-cell movement occurred from 87 to 100% of the regular invaded

Figure 5. (continued).

(top left corner). Images presented here, and in **(D)**, were acquired with long exposure times (10 s for EGFP and 6 s for mRFP) for visualization of faint fluorescence in the rice cytoplasm. With reduced exposure times, BAS4:EGFP uniformly outlined IH (see Supplemental Figure 6F online).

(D) PWL2:EGFP (green), but not BAS4:mRFP (red), was observed in the cytoplasm of rice cells invaded by KV105 (27 HAI) and in adjoining rice cells. Note that there is some cell wall autofluorescence in both the mRFP and EGFP images. Exposure times were 10 s for EGFP and 6 s for mRFP.

(E) BAS1:mRFP (red) was observed in the cytoplasm of cells invaded by KV96, as well as in surrounding cells, here imaged at 36 HAI as described in **(B)** to **(D)**. Asterisks indicate rice cells with IH and plus signs indicate rice cells without IH. Exposure time for mRFP was 1.5 s. Merge shows DIC and mRFP.

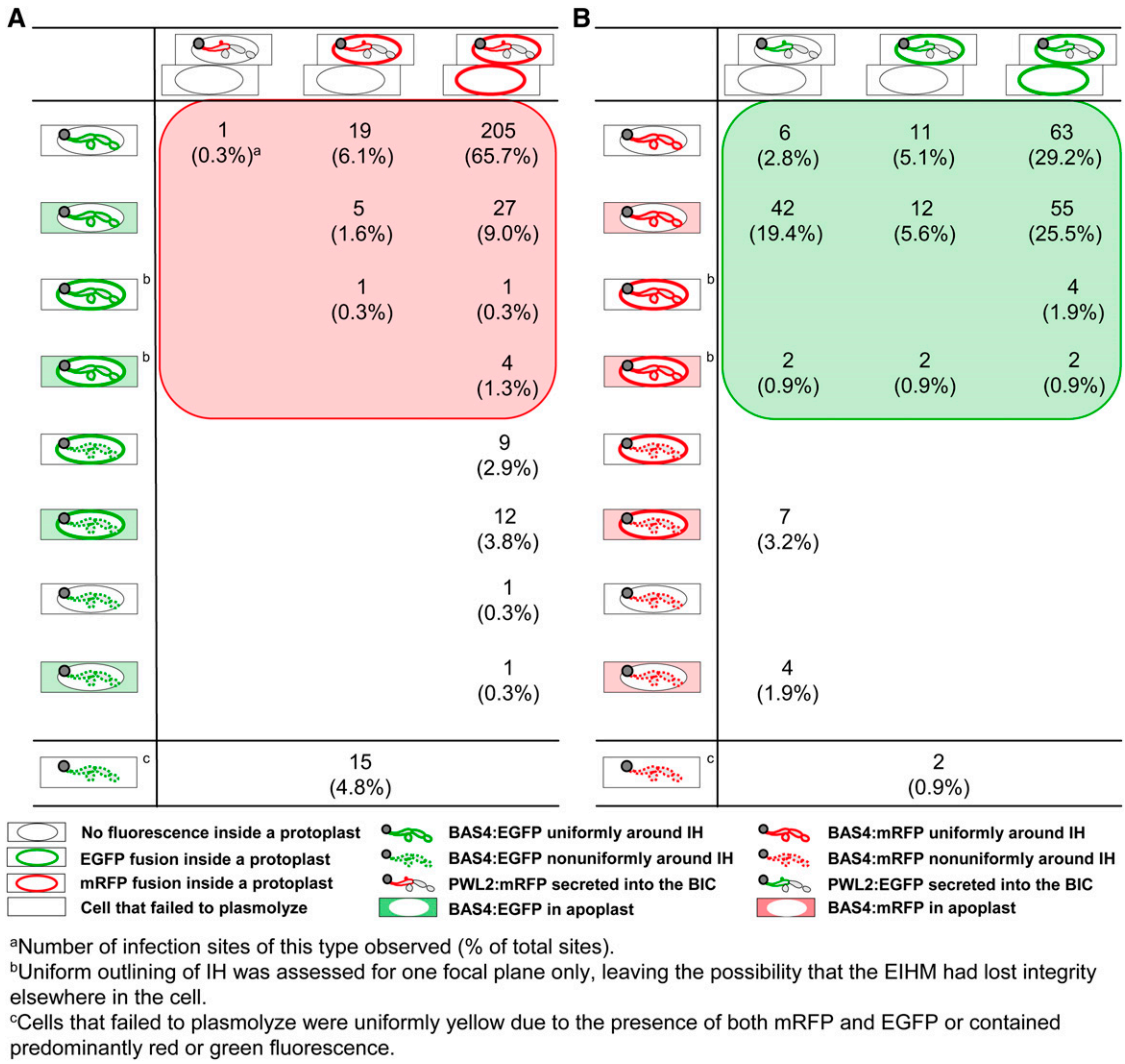

[a]Number of infection sites of this type observed (% of total sites).
[b]Uniform outlining of IH was assessed for one focal plane only, leaving the possibility that the EIHM had lost integrity elsewhere in the cell.
[c]Cells that failed to plasmolyze were uniformly yellow due to the presence of both mRFP and EGFP or contained predominantly red or green fluorescence.

Figure 6. Quantitative Analysis of Translocation of PWL2:FP, but Not BAS4:FP, into the Host Cytoplasm.

Schematic diagrams illustrate different fluorescence patterns of fusion proteins secreted from IH expressing PWL2:mRFP and BAS4:EGFP **(A)** (represented here are 301 out of a total of 312 infection sites) and PWL2:EGFP and BAS4:mRFP **(B)** (represented here are 212 out of a total of 216 infection sites). Rectangles represent rice cells, and ovals represent the plasmolyzed rice protoplast. For PWL2:FP patterns, both the invaded and immediate neighbors were illustrated to indicate cell-to-cell movement of translocated PWL2:FP. For BAS4:FP patterns, only the invaded cell was illustrated. BAS4:FP was not observed in adjoining cells except in a subset of the few cases in which BAS4:FP had apparently reached the host cytoplasm by spillage from damaged EIHM. The shaded red box in **(A)** and the shaded green box in **(B)** indicate the successful infection sites with plasmolysis and uniform BAS4-outlining of IH.

epidermal cells (Figure 7B). Clearly, movement of translocated PWL2:mRFP to adjoining host cells depended on cell type.

Cell-to-cell movement also appeared to depend on the size of the translocated protein. Replacing mRFP with the brighter tdTomato at the C terminus of PWL2 facilitated observation of translocation into the cytoplasm of invaded host cells (n = 25). However, compared with the frequent cell-to-cell movement observed for PWL2:mRFP (39.3 kD), the larger PWL2:tdTomato (68.3 kD) was rarely observed in adjoining uninvaded rice cells (Figure 5B). To confirm that the size of the fusion protein had an impact, we compared cell-to-cell movement of the host nuclear-localized PWL2 fusion proteins based on easily countable fluorescent nuclei (Table 1). Fluorescence from the smaller PWL2:mCherry:NLS (44.5 kD) exhibited cell-to-cell movement in all 29 regular invaded cells examined, and mCherry fluorescence had moved more than two cells away from the invaded cells in 93% of these sites (Table 1). By contrast, movement of the larger PWL2:hH1:mCherry protein (66.1 kD) out of regular invaded epidermal cells was limited. Very weak fluorescence was seen only in immediate neighboring cells in 87% of infection sites, and no movement was seen in the remaining 13%. Comparison of fluorescence patterns for PWL2:mRFP (39.3 kD), PWL2:EGFP

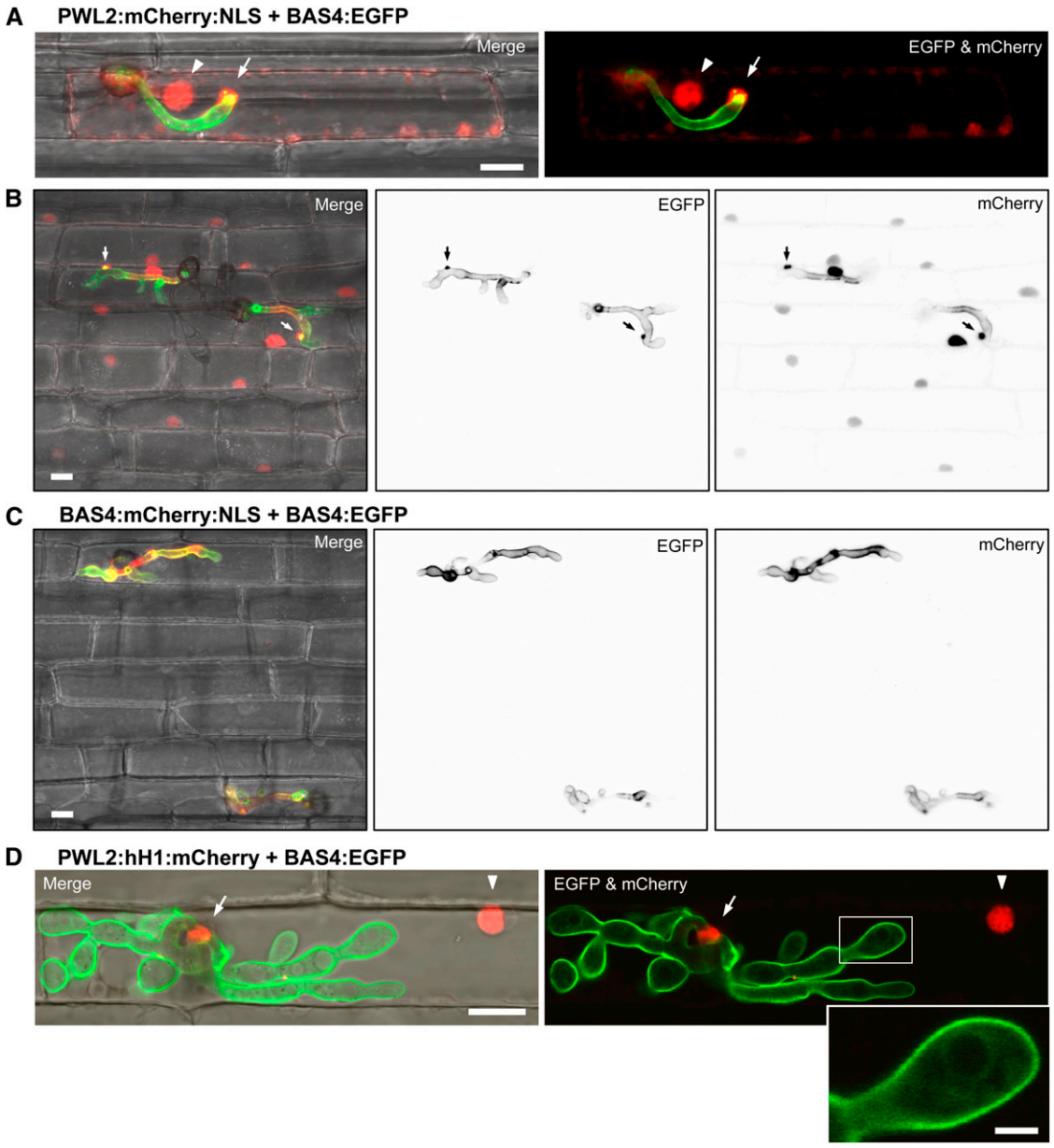

Figure 7. Nuclear Targeting of PWL2:mCherry Facilitates Visualization of Effector Translocation and Cell-to-Cell Spread.

Transformants expressing fluorescently labeled PWL2 and BAS4 proteins in YT16 rice are shown as projections of confocal optical sections taken at 0.45-μm z-intervals over a depth of 21.7 μm **(A)** or 18.53 μm (**[B]** and **[C]**), or as a single-plane confocal image **(D)**. Merge shows bright-field, EGFP, and mCherry. Arrows indicate BICs, arrowheads indicate rice nuclei, and yellow indicates overlapping EGFP and mCherry fluorescence signals. NLS, three tandem repeats of the nuclear localization signal from simian virus large T-antigen; hH1, histone protein H1 of *N. crassa.* Bars = 10 μm except in inset of **(D)**.

(A) and **(B)** Transformant KV121 expressing PWL2:mCherry:NLS (red) and BAS4:EGFP (green) at 30 HAI.

(A) mCherry fluorescence was observed in the primary hyphal tip BIC and in the nucleus of this vein-associated rice cell, but not in adjoining cells. Faint mCherry fluorescence was also seen in an ER-like network inside the invaded rice cell. Pinhole settings were 2 airy units for EGFP and 3 airy units for mCherry.

(B) Bright PWL2:mCherry:NLS fluorescence occurred in the nuclei of invaded cells. Lower levels of fluorescence occurred in nuclei of surrounding cells (all 11 in this image). Single-channel images of EGFP or mCherry fluorescence are shown in black and white. Pinhole settings were 1 airy unit for EGFP and 3 airy units for mCherry. The same imaging conditions were used in **(C)** and in the autofluorescence control (see Supplemental Figure 6C online).

(C) Fluorescence from BAS4:mCherry:NLS (red) was not observed in rice nuclei; instead, it outlined the IH together with BAS4:EGFP (green). Transformant KV122 at 30 HAI imaged as described in **(B)**.

(D) PWL2:hH1:mCherry (red), but not BAS4:EGFP (green), was observed in the BIC and the nucleus of the cell invaded by KV123 at 28 HAI in this single-plane confocal image obtained with optimal pinhole settings. Note BAS4:EGFP fluorescence outlining the IH and the distinctive green, but not red, fluorescence inside the IH (inset; bar = 2.5 μm), presumably representing BAS4:EGFP in the process of secretion.

Table 1. Cell-to-Cell Movement of PWL2 Fusion Proteins after Translocation into First-Invaded Cells at 26 to 30 HAI

Protein Expressed from the Fungus[a]	Size (kD)[b]	Cell Type[c]	Number of Infection Sites Analyzed[d]	Cell-to-Cell Movement[e]		No Movement[f]
				Adjacent Cells Only	More Than Two Cells	
PWL2:mCherry:NLS	44.5	Regular	29	2 (6.9%)	27 (93.1%)	0
		Vein-associated	12	1 (8.3%)	0	11 (91.7%)
PWL2:hH1:mCherry	66.1	Regular	78	68[g] (87.2%)	0	10 (12.8%)
		Vein-associated	25	2 (8.0%)	0	23 (92.0%)

[a]Entire PWL2 protein was expressed under control of the native promoter with C-terminal fusions of nuclear targeting mCherry. NLS, three tandem repeats of the nuclear localization signal from simian virus large T-antigen; hH1, histone H1 from *N. crassa*.
[b]Estimated size of mature PWL2 fusions without the signal peptide.
[c]Regular or vein-associated cells in rice sheath epidermal tissue.
[d]Infection sites combined from at least two independent experiments.
[e]Fluorescence was observed in nuclei of rice cells immediately adjacent to the invaded cell or more than two cells away from the invaded cell.
[f]Fluorescence was observed only in invaded cells, predominantly in nuclei.
[g]Fluorescence was extremely weak in cells immediately adjacent to the invaded cell compared to fluorescence in the invaded cell.

(40.9 kD), and PWL2:mCherry:NLS (44.5 kD) with patterns for PWL2:hH1:mCherry (66.1 kD) and PWL2:tdTomato (68.3 kD) suggested that there is an upper size limit for host cell-to-cell movement, but, with the range of proteins tested, not for translocation into host cells.

DISCUSSION

A Novel Interfacial Structure Associated with Rice Blast Disease

Our study adds detail to the dynamic events leading to the biotrophic association between *M. oryzae* and rice cells. We describe development of the BIC, a novel structure that accumulates AVR effectors and the BAS1 protein during the key decision period between disease compatibility and hypersensitive resistance. The first stage of BIC development corresponds to the EIHM membranous cap reported by Kankanala et al. (2007) to extend in front of primary or filamentous IH hyphal tips (summarized in Figure 1E). Chimeric fluorescent AVR-Pita1, PWL1, PWL2, and BAS1 show extensive accumulation in tip BICs soon after initial host cell invasion. By contrast, fluorescent BAS4 protein brightly outlines the primary hyphae and appears as an inner layer in the BIC (Figure 7A). The tip BIC is associated with rice cytoplasm that is dynamically tethered to the appressorial penetration region (Figure 2A). Continuing connection between the growing hyphal tip and the penetration region is consistent with the characteristic growth reorientation in the compatible interaction (see examples in Figures 1B and 2), which was first noted by Heath and colleagues (1990). Using our most sensitive translocation assay, we demonstrated that fluorescent effectors were translocated into invaded host cells at the earliest stage of cell invasion when primary hyphae were growing and effectors were accumulating in tip BICs (Figure 7A).

The second stage of BIC development corresponds to the critical disease event in which filamentous primary hyphae (parallel-sided unconstricted true hyphae) differentiate into bulbous IH (pseudohyphae with obvious constrictions at septal sites) (Heath et al., 1990; Veses and Gow, 2009). When this happens, the tip BIC becomes the distinctive structure beside the first IH cell (Figures 1C to 1E; see Supplemental Movie 1 online). The leaving behind of the tip BIC after hyphal differentiation confirmed that membrane caps were not associated with bulbous IH (Kankanala et al., 2007). While the fungus grew in a host cell, fluorescent effector proteins localized in the BIC and around the BIC-associated cells, namely, the primary hypha and first IH cell. PWL2:EGFP continued to accumulate in the BIC after differentiation, while IH were growing elsewhere (Figure 3). Subsequently formed IH cells, including cells that branch from primary hyphae (Figures 1B and 3), secreted BAS4:FP, and this small Cys-rich protein was not translocated to the host cytoplasm (Figures 5 to 7). Faint BAS4:EGFP fluorescence inside non-BIC IH cells presumably corresponded to BAS4 in the process of being secreted, but similar PWL2 fluorescence was not observed in these cells (Figure 7D, inset). When PWL2 fluorescence was observed in non-BIC IH cells, it appeared in presumptive vacuoles (Figure 1B). Clearly, BIC-associated hyphal cells are differentiated from subsequently formed IH cells by their strong association with secreted effectors.

The importance of effector accumulation in BICs to the compatible interaction is highlighted by the general absence of fluorescent effectors in BICs in the incompatible interaction (Mosquera et al., 2009; Yi et al., 2009). Although faint fluorescence from effector:FPs was sometimes observed in cells undergoing *R* gene–mediated HR, fully developed fluorescent BICs were not observed. By contrast, straight hyphae in the incompatible interaction either failed to grow or continued growing perpendicularly into underlying mesophyll cells (Heath et al., 1990; Mosquera et al., 2009). The correlations between preferential accumulation of effectors in BICs and compatible interactions and between preferential BIC accumulation and effector translocation together support our working hypothesis that the BIC represents the site of effector translocation in rice blast disease.

The next step in demonstrating a role for BICs in effector translocation lies in identifying the precise sequence motifs that regulate preferential BIC accumulation and in demonstrating that these motifs also impact host translocation. The critical sequences appear to reside somewhere within the promoter through signal peptide-encoding sequences. That is, AVR-Pita1, PWL1, and PWL2 promoter/signal peptide sequences mediate BIC

localization of EGFP in a manner characteristic of intact effectors (Figures 1C and 1D; see Supplemental Figure 3A online). The BAS4 promoter/signal peptide (see Supplemental Figure 5 online; Mosquera et al., 2009) and P27 promoter/CUT1 signal peptide (Figure 4) mediate outlining of non-BIC-associated IH and minimal BIC localization. Therefore, preferential BIC accumulation might be explained by enhanced expression of effector genes in BIC-associated cells, by a specialized effector secretion process in these cells (Shoji et al., 2008) or by some combination of both. Alternatively, 5′-mRNA sequences might mediate preferential BIC accumulation. Our finding that FPs expressed with the *PWL1*, *PWL2*, and *AVR-Pita1* promoters were uniformly distributed in the IH cytoplasm (Figure 1A; see Supplemental Figure 3A online) suggested that these promoters were expressed in all IH cells. However, we cannot rule out a role for differential effector expression because it remains possible that proteins that are highly expressed in BIC-associated cells are redistributed throughout the IH by cytoplasmic streaming through septal pores.

At least initially, AVR-Pita1 appears to be secreted into BICs using the normal fungal ER-mediated secretion machinery because mutation in the ER chaperone LHS1 with a role in secretion severely impairs its BIC accumulation and its function in triggering Pita-mediated HR (Yi et al., 2009). Another study suggested that *M. oryzae* uses different secretion mechanisms in planta because the *APT2* gene, which encodes a Golgi-localized P-type ATPase, appears to only be involved in secretion of the tested AVR effector and a subset of extracellular enzymes (Gilbert et al., 2006). N-terminal signal sequences, though seemingly highly conserved in function, can specify diverse targeting pathways, determine efficiency of translocation, and even have postcleavage functions (Hegde and Bernstein, 2006; Cross et al., 2009). Understanding in planta secretion pathways that might diverge after initial ER entry remains a high priority.

Since the first hyphae that grow in host cells exhibit typical filamentous growth (Figure 1E), standard hyphal tip secretion mechanisms (Steinberg, 2007; Shoji et al., 2008) could account for delivery of effector:FPs into apical BICs. Effector:FP continued to accumulate in BICs that have been left behind by growing bulbous IH (Figure 3), raising the possibility that the original apical secretion apparatus was maintained adjacent to the BIC besides the IH cell. However, we cannot currently eliminate the possibility that effector:FPs are secreted elsewhere and accumulate in BICs through some unknown mechanism. Fluorescent labeling of components of the standard fungal secretion machinery, the spitzenkörper and polarisome (Steinberg, 2007; Shoji et al., 2008), will begin to answer questions on mechanisms of secretion and BIC accumulation, as well as questions on location and mechanism for secretion of proteins such as BAS4 that do not show preferential BIC localization.

For the eukaryotic pathogens, specific cellular structures that appear to function in translocation of secreted effectors to the host cytoplasm have only been identified for the malaria parasite. *P. falciparum* is contained within a parasitophorous vacuole inside red blood cells, and pathogen-induced Maurer's Clefts, lamellar membrane structures in the host cytoplasm, have been associated with effector trafficking to host cytosol and membranes (Bhattacharjee et al., 2008). Alternatively, it has been reported that oomycete effectors are translocated to the host cytoplasm without pathogen-induced or encoded machinery (Dou et al., 2008). For fungal and oomycete plant pathogens, extensive ultrastructural studies have identified complex features at the interfaces between haustoria and the host cytoplasm, including tubular elements extending into the plant cytoplasm from the extrahaustorial membranes and signs of vesicular activity at the interface (Mims et al., 2004; O'Connell and Panstruga, 2006). Other biotrophic fungi, including smut fungi, produce a membranous, extracellular interaction apparatus inside the fungal cell wall, which is connected to an interaction zone enclosed by invaginated plasma membrane in the host cell (Simon et al., 2004; Mims and Richardson, 2007). Detailed ultrastructural analyses of BICs coupled with immunogold localization of effectors should provide insight into the potential role for BICs in effector translocation.

Translocation of Cytoplasmic Blast Effectors into Rice Cells

Although translocation motifs have been suggested, fungal effectors do not contain highly conserved, easily recognizable amino acid motifs (Ellis et al., 2007; Kamoun, 2007) such as the RxLxE/Q/D motif in *P. falciparum* effectors or the RXLR-dEER motif in oomycete plant pathogens (Bhattacharjee et al., 2006; Dou et al., 2008). Using live-cell imaging of fluorescent reporter proteins in rice leaf sheaths, we developed a robust assay for cytoplasmic effector translocation that will facilitate mutational approaches for motif identification. Previously, Whisson et al. (2007) demonstrated that an AVR effector from *Phytophthora infestans* was translocated into potato leaf cells using the enzymatic β-glucuronidase reporter to amplify the signal. Mutation of the oomycete translocation motif RXLR-dEER eliminated this translocation. Kemen et al. (2005) detected a haustorium-secreted protein, *Uf*-RTP1p, in nuclei of invaded host cells by immunolocalization, but mutational analysis is difficult for the obligate pathogen *Uromyces fabae*. Our fluorescent translocation signal in the rice cytoplasm is faint, especially compared with bright BIC fluorescence (Figures 5C and 5D; see Supplemental Figure 6 online). Visualization of effector translocation was facilitated using brighter fluorescent protein variants tdTomato and mCherry and by concentration of the translocated FP, either by plasmolysis or by targeting to host nuclei. The nuclear targeting-based translocation assay provides several advantages: (1) no need for plasmolysis; (2) detection sensitive enough to visualize host translocation of effectors secreted by primary hyphae (Figure 7A); (3) detection sensitive enough to observe translocation with optimal pinhole settings in confocal microscopy, especially with the PWL2:hH1:mCherry accumulating mainly in the infected cell (Figure 7D); and (4) ease of observation of movement of fluorescent PWL2 protein into rice nuclei in surrounding cells (Figure 7B). With this assay, our top priority is to identify the still elusive translocation motif, if any, for rice blast effectors. Such a motif would become a valuable resource for identifying sets of putative effectors by bioinformatic analyses, as has been true for the malarial and oomycete pathogens (Bhattacharjee et al., 2006; Whisson et al., 2007; Jiang et al., 2008).

In fully compatible infection sites, bright BAS4:EGFP fluorescence was observed in the EIHM compartment without apparent diffusion into the host cell wall (apoplast). Although it is generally

accepted that low pH in the plant apoplast is not conducive to GFP fluorescence (Zheng et al., 2004), we have the same results with mRFP and mCherry, which are easily observed in the apoplast (Whisson et al., 2007; Doehlemann et al., 2009). Indeed, if the rice sheath apoplast is not compatible with EGFP, this suggests that the EIHM compartment and the bulk apoplast are distinct environments and supports our working hypothesis that there is not an open connection between these two spaces. On the other hand, faint BAS4 fluorescence (compared with strong EIHM matrix fluorescence) was observed in the apoplastic space between the rice cell wall and the shrunken protoplast in a number of plasmolyzed infection sites that are successful according to our criteria of uniform BAS4-outlining and an intact rice plasma membrane (Figure 6; see Supplemental Figures 6F and 6G online). This leads to the question of whether this is artifactual leakage or whether the intracellular IH have a separate translocation route to deliver effectors extracellularly. Compared with PWL2 (2 Cys) and BAS1 (0 Cys), BAS4 is Cys rich (8 Cys), which is a characteristic property of apoplastic effectors (Kamoun, 2006). Identification of additional BAS proteins with EIHM matrix accumulation will determine if this is a general phenomenon.

Effector Movement Precedes Fungal Growth

Kankanala et al. (2007) noticed that the blast fungus spends ~12 h in first invaded cells, but it moves through subsequently invaded cells in ~2 h. They suggested that IH in this first-invaded cell might be sending signals ahead to prepare neighboring host cells before entering them, possibly through plasmodesmata. Our current results on movement of PWL2 and BAS1 FPs into neighboring cells preceding IH growth support this hypothesis. Proteins in the plant cytoplasm can move through the cytoplasmic sleeve in plasmodesmata through targeted or nontargeted mechanisms (Oparka et al., 1999; Zambryski, 2004). Viral movement proteins show targeted movement, which is associated with punctate plasmodesmatal localization patterns. By contrast, proteins in the plant cytoplasm can move by nontargeted mechanisms in which plasmodesmata appear to exist in a dilated state. The dilation state of plasmodesmata in particular plant cells depends on leaf age, cell type, environment, and whether tissues are serving as a sink (importing photosynthate) or as a source (exporting photosynthate). In tobacco (*Nicotiana tabacum*) source tissue, GFP (26.9 kD) rarely traffics to surrounding cells. However, in sink tissue, proteins that are ~50 kD move to form multicellular fluorescent foci surrounding the expressing cells (Oparka et al., 1999). In our system, movement of PWL2:FPs to adjoining cells depends on cell type (regular versus vascular-associated epidermal cells) and on size of the fusion protein, which is consistent with trafficking of blast effectors through plasmodesmata. If PWL2 and BAS1 FPs do move through plasmodesmata, they would appear to use nontargeted mechanisms, since they do not show a predominantly punctate plasmodesmatal pattern. The mechanism of blast effector cell-to-cell trafficking remains to be determined.

Our results present biological insights into the degree of biotrophy involved in rice blast disease. Fluorescently labeled proteins PWL2 and BAS1 were observed to have moved up to four host cells ahead while the fungus was still growing in the first-invaded rice cells (Figures 5C, 5E, and 7B; see Supplemental Figure 6D online). This suggests that successfully invaded rice cells remain in symplastic continuity with surrounding cells and that these surrounding rice cells are already responding to the effectors, perhaps by expressing rice genes that contribute to disease susceptibility. Recently, Mosquera et al. (2009) used the same hand-trimming procedure we used for microscopy to purify rice sheath tissue that was enriched for first-invaded rice cells and their immediate neighbors. The IH growing in these tissues were expressing many novel *BAS* genes, including *PWL2* and *BAS1*. This analysis also identified candidate effector-triggered susceptibility genes that remain to be investigated. Additionally, with our constructed nuclear-targeting fluorescent effectors, we obtained detailed images documenting random nuclear locations in invaded rice cells. It is an exciting possibility that IH secretion studies with additional BAS proteins will provide further insight into blast biotrophic invasion and effector functions.

METHODS

Strains, Plasmids, and Fungal Transformation

Magnaporthe oryzae wild-type strains and transformants are described in Supplemental Table 1 online. Effector:EGFP expression plasmids were constructed by PCR amplifying different effector gene regions and fusing them to the N terminus of EGFP. For *AVR-Pita1*, these include promoter alone, promoter and sequence encoding 21 amino acids containing the signal peptide, promoter and 47–amino acid predicted prepropeptide coding sequence sequence, and promoter with the entire 223–amino acid coding sequence. For *PWL1* and *PWL2*, these include each promoter alone, each promoter and the 21–amino acid signal sequence, and each promoter with its entire 147– and 145–amino acid coding sequence, respectively. The *PWL2* promoter and its entire 145–amino acid coding sequence were also fused to mRFP, tdTomato, or nuclear targeting mCherry (mCherry:NLS and hH1:mCherry). The *BAS4* promoter and its entire 102–amino acid coding sequence were fused to EGFP, mRFP, or nuclear targeting mCherry:NLS. The *M. oryzae* ribosomal protein 27 (P27) promoter was used to construct constitutive expression plasmids for cytoplasmic EGFP, for secreted CUT1:EGFP or for in vitro secretion of the AVR-Pita1:EGFP fusion. The EGFP gene was obtained from Clontech, the mRFP gene was from Campbell et al. (2002), and the tdTomato and the mCherry genes (Shaner et al., 2008) were isolated from pAN582 and pAN583, respectively (Nelson et al., 2007). Nuclear targeting reporters were constructed by cloning NLS (three tandem repeats of the nuclear localization signal from simian virus large T-antigen) or hH1 (histone H1 from *Neurospora crassa*) at the C or N terminus of mCherry, respectively. NLS was isolated from pEBFP2-Nuc (Ai et al., 2007) (Addgene plasmid 14893) and hH1 from pAM1293 obtained from Marc Orbach (University of Arizona). All the fusion constructs were cloned in binary vectors pBHt2 (Mullins et al., 2001) or pBGt (S. Kang, unpublished data), and their transcriptional and translational fusions were verified by DNA sequencing. See Supplemental Methods online for details of plasmid construction, Supplemental Table 2 online for PCR primers used, and Supplemental Table 3 online for the list of plasmids used.

Plasmids were transformed into laboratory strains CP987 (*avr-pita1*$^-$ *pwl1*$^-$ *pwl2*$^-$), 4091-5-8 (*avr-pita1*$^-$ *pwl1*$^-$ *pwl2*$^-$), field isolates O-137 (*AVR-Pita1 PWL2*) (Valent et al., 1991), and/or Guy11 (*avr-pita1*$^-$) (Leung et al., 1988) using *Agrobacterium tumefaciens*–mediated transformation (Khang et al., 2006). Because positive transformants showed similar fluorescence patterns with varying intensities, those with strongest fluorescence were studied (see Supplemental Table 1 online).

Infection Assays

Rice (*Oryza sativa*) cultivars Yashiro-mochi (YM, *Pita*/*Pita*) and YT16 (*pita*$^{-}$/*pita*$^{-}$) and weeping lovegrass (*Eragrostis curvula*) were used for whole-plant infections as described (Kang et al., 1995; Berruyer et al., 2006). Leaf sheath inoculation was performed by incubating fungal spores (2×10^4 spores/mL in 0.25% gelatin) in the hollow interior of detached rice leaf sheaths, and the inner epidermal layer was excised for microscopy (Kankanala et al., 2007). The assay for in vitro secretion by IH-like hyphae (Bourett and Howard, 1990) is described in the Supplemental Methods online.

Microscopy

Conventional epifluorescence and differential interference contrast (DIC) microscopy was performed on a Zeiss Axioplan 2 IE MOT microscope using 63×/1.2 numerical aperture (NA) C-Apochromat water immersion and 40×/0.75 NA EC Plan Neofluar objectives. Images were obtained with an Axiocam HRc camera and Axiovision software version 4.6. Unless stated otherwise, microscopy components were obtained from Carl Zeiss. Fluorescence was observed with a 100-W FluoArc or an X-Cite 120 (EXFO Life Sciences) mercury lamp source. Filter sets used were as follows: EGFP (excitation 480 ± 10 nm, emission 510 ± 10 nm, filter set 41020; Chroma Technology); YFP (excitation 500 ± 20 nm, emission 535 ± 30 nm, filter set 46); and mRFP and tdTomato (excitation 535 ± 25 nm, emission 610 ± 32 1/2 nm).

Confocal microscopy was performed on a Zeiss Axiovert 200M microscope equipped with a Zeiss LSM 510 META system using 40×/1.2 NA and 63×/1.2 NA C-Apochromat water immersion objectives. Excitation/emission wavelengths were 488 nm/505 to 550 nm for EGFP and 543 nm/560 to 615 nm for tdTomato, mRFP, and mCherry. Images were acquired and processed using LSM 510 AIM version 4.2 SP1 software.

FRAP

Experiments were performed using a Zeiss LSM 510 confocal microscope with a 30.0-mW 488-nm argon laser and a C-Apochromat 63×/1.2NA water immersion objective at 6× optical zoom. A region containing a fluorescent BIC and BIC-associated cells was identified in a YT16 rice sheath epidermal cell invaded by transformant KV105 expressing PWL2:EGFP. For FRAP analyses, a specific region of interest (ROI) that covered the entire fluorescence of the BIC was selected for bleaching. Twenty bleaching iterations were performed at 100% laser power. These bleaching conditions were empirically determined to reduce the fluorescent signal of the photobleached ROI to <10% of the prebleach intensity. Image scans were taken with the acousto-optic tunable filter attenuated to 5% laser power immediately before and after bleaching and then approximately every 20 min for up to 3 h. During the course of imaging, the BIC shifted in focus or position as a result of differentiation of BIC-associated cells. Prior to image acquisition of each recovery time point, such movement of the BIC or focal plane was corrected manually so that the brightest BIC fluorescence was imaged. For quantitative analyses, BIC fluorescence recovery curves were measured as the mean intensity of ROI pixels using the LSM 510 software (version 4.2 SP1), normalized, and plotted using Microsoft Excel.

Plasmolysis-Based Assay for Visualization of Fluorescence in the Rice Cytoplasm

Rice cells were plasmolyzed immediately before microscopy to concentrate the cytoplasm and separate it from the cell walls. Plasmolysis was performed slowly, by sequential incubation of the rice tissue in 0.25, 0.50, and 0.75 M sucrose. This gradual plasmolysis minimizes damage to the host cells (Mellersh and Heath, 2001). Microscopy was performed on a Zeiss Axioplan 2 IE MOT microscope as described above. Fluorescence images were acquired using the Axiovision software module Multichannel Fluorescence with a series of incremental exposure times (1, 2, 3, and 4 s for EGFP, and 0.3, 1, 2, and 3 s for mRFP or tdTomato). Acquired images for each fluorescence channel were examined separately or combined in single images to produce the maximum exposure images (10 s for EGFP and 6.3 s for mRFP or tdTomato) sometimes required for visualizing fluorescence in the rice cytoplasm. Images obtained at the reduced exposure times were valuable for assessing uniform outlining of IH by BAS4:FP and localized BIC secretion by PWL2 (or BAS1):FP.

Accession Numbers

Sequence data from this article can be found in the GenBank/EMBL databases under the following accession numbers: AF207841 for *AVR-Pita1*, U26313 for *PWL2*, AB480169 for *PWL1*, FJ807764 for *BAS1*, FJ807767 for *BAS4*, XM_365241 for *CUT1*, and AY142483 for *M. oryzae* ribosomal protein 27 promoter.

Supplemental Data

The following materials are available in the online version of this article.

Supplemental Figure 1. Graphic Presentation of the *AVR-Pita1*, *PWL1*, and *PWL2* Genes and the EGFP Fusion Constructs Used in This Study.

Supplemental Figure 2. The EGFP Fusion Proteins Containing the Entire Coding Sequences of *AVR-Pita1*, *PWL1*, or *PWL2* Still Function in Conferring Host Specificity.

Supplemental Figure 3. In Planta Secretion of Effector:EGFP Fusion Proteins into BICs.

Supplemental Figure 4. AVR-Pita1 Signal Peptide Mediates EGFP Secretion in Vitro.

Supplemental Figure 5. Comparison of the *BAS4* Signal Peptide-Encoding Sequence with the Entire Coding Sequence for Targeting EFGP to the EIHM Matrix.

Supplemental Figure 6. Images of Autofluorescence Controls and of Localization of PWL2:FP and BAS4:FP at Individual Infection Sites.

Supplemental Table 1. Fungal Strains Used in This Study.

Supplemental Table 2. PCR Primers Used in This Study.

Supplemental Table 3. Key Plasmids Used in This Study.

Supplemental Movie 1. A Membranous Cap Moves BIC Moves to Form the BIC Body Beside the Differentiating IH Cell.

Supplemental Movie 2. Dynamic Movement of a Cytoplasmic Strand Connecting the Tip of a Primary Hypha to Cytoplasm at the Appressorial Penetration Site.

Supplemental Methods.

Supplemental Movie Legends.

ACKNOWLEDGMENTS

We thank Dr. Gurdev S. Khush (University of California, Davis) for his support and encouragement during the course of this project. We thank Melinda Dalby and Britni Samuelson for their excellent technical support and Marsha Landis for assistance in preparing figures. We thank Philine Wangemann and Joel Sanneman at Kansas State University for excellent technical support in confocal microscopy. This work was initiated

under USDA–National Research Initiative Grants 2002-35319-12567 to B.V. and 2005-35319-15310 to S.K. and continued under 2006-35319-17296 to B.V. We acknowledge generous support from the COBRE Confocal Microfluorometry and Microscopy Core at Kansas State University, funded by National Institutes of Health Grant P20 RR-017686. This is contribution 10-272-J from the Agricultural Experiment Station at Kansas State University.

Received July 14, 2009; revised March 11, 2010; accepted April 14, 2010; published April 30, 2010.

REFERENCES

Ai, H.-W., Shaner, N.C., Cheng, Z., Tsien, R.Y., and Campbell, R.E. (2007). Exploration of new chromophore structures leads to the identification of improved blue fluorescent proteins. Biochemistry **46:** 5904–5910.

Ballini, E., Morel, J.-B., Droc, G., Price, A., Courtois, B., Notteghem, J.-L., and Tharreau, D. (2008). A genome-wide meta-analysis of rice blast resistance genes and quantitative trait loci provides new insights into partial and complete resistance. Mol. Plant Microbe Interact. **21:** 859–868.

Berruyer, R., Poussier, S., Kankanala, P., Mosquera, G., and Valent, B. (2006). Quantitative and qualitative influence of inoculation methods on in planta growth of rice blast fungus. Phytopathology **96:** 346–355.

Bhattacharjee, S., Hiller, N.L., Liolios, K., Win, J., Kanneganti, T.-D., Young, C., Kamoun, S., and Haldar, K. (2006). The malarial host-targeting signal is conserved in the Irish potato famine pathogen. PLoS Pathog. **2:** e50.

Bhattacharjee, S., van Ooij, C., Balu, B., Adams, J.H., and Haldar, K. (2008). Maurer's clefts of *Plasmodium falciparum* are secretory organelles that concentrate virulence protein reporters for delivery to the host erythrocyte. Blood **111:** 2418–2426.

Bhavsar, A.P., Guttman, J.A., and Finlay, B.B. (2007). Manipulation of host-cell pathways by bacterial pathogens. Nature **449:** 827–834.

Böhnert, H.U., Fudal, I., Dioh, W., Tharreau, D., Notteghem, J.-L., and Lebrun, M.-H. (2004). A putative polyketide synthase/peptide synthetase from *Magnaporthe grisea* signals pathogen attack to resistant rice. Plant Cell **16:** 2499–2513.

Bourett, T.M., and Howard, R.J. (1990). *In vitro* development of penetration structures in the rice blast fungus *Magnaporthe grisea.* Can. J. Bot. **68:** 329–342.

Bryan, G.T., Wu, K., Farrall, L., Jia, Y., Hershey, H.P., McAdams, S.A., Faulk, K.N., Donaldson, G.K., Tarchini, R., and Valent, B. (2000). A single amino acid difference distinguishes resistant and susceptible alleles of the rice blast resistance gene *Pi-ta.* Plant Cell **12:** 2033–2045.

Campbell, R.E., Tour, O., Palmer, A.E., Steinbach, P.A., Baird, G.S., Zacharias, D.A., and Tsien, R.Y. (2002). A monomeric red fluorescent protein. Proc. Natl. Acad. Sci. USA **99:** 7877–7882.

Couch, B.C., Fudal, I., Lebrun, M.-H., Tharreau, D., Valent, B., van Kim, P., Notteghem, J.-L., and Kohn, L.M. (2005). Origins of host-specific populations of the blast pathogen *Magnaporthe oryzae* in crop domestication with subsequent expansion of pandemic clones on rice and weeds of rice. Genetics **170:** 613–630.

Cross, B.C.S., Sinning, I., Luirink, J., and High, S. (2009). Delivering proteins for export from the cytosol. Nat. Rev. Mol. Cell Biol. **10:** 255–264.

Dean, R.A., et al. (2005). The genome sequence of the rice blast fungus *Magnaporthe grisea.* Nature **434:** 980–986.

Doehlemann, G., van der Linde, K., Aßmann, D., Schwammbach, D., Hof, A., Mohanty, A., Jackson, D., and Kahmann, R. (2009). Pep1, a secreted effector protein of *Ustilago maydis* is required for successful invasion of plant cells. PLoS Pathog. **5:** e1000290.

Dou, D., Kale, S.D., Wang, X., Jiang, R.H.Y., Bruce, N.A., Arredondo, F.D., Zhang, X., and Tyler, B.M. (2008). RXLR-mediated entry of *Phytophthora sojae* effector Avr1b into soybean cells does not require pathogen-encoded machinery. Plant Cell **20:** 1930–1947.

Ebbole, D.J. (2007). Magnaporthe as a model for understanding host-pathogen interactions. Annu. Rev. Phytopathol. **45:** 437–456.

Ellis, J., Catanzariti, A.M., and Dodds, P. (2006). The problem of how fungal and oomycete avirulence proteins enter plant cells. Trends Plant Sci. **11:** 61–63.

Ellis, J.G., Dodds, P.N., and Lawrence, G.J. (2007). Flax rust resistance gene specificity is based on direct resistance-avirulence protein interactions. Annu. Rev. Phytopathol. **45:** 289-306.

Farman, M.L., and Leong, S.A. (1998). Chromosome walking to the *AVR1-CO39* avirulence gene of *Magnaporthe grisea*. Discrepancy between the physical and genetic maps. Genetics **150:** 1049–1058.

Gilbert, M.J., Thornton, C.R., Wakley, G.E., and Talbot, N.J. (2006). A P-type ATPase required for rice blast disease and induction of host resistance. Nature **440:** 535–539.

Heath, M.C., Valent, B., Howard, R.J., and Chumley, F.G. (1990). Interactions of two strains of *Magnaporthe grisea* with rice, goosegrass, and weeping lovegrass. Can. J. Bot. **68:** 1627–1637.

Hegde, R.S., and Bernstein, H.D. (2006). The surprising complexity of signal sequences. Trends Biochem. Sci. **31:** 563–571.

Jia, Y., McAdams, S.A., Bryan, G.T., Hershey, H.P., and Valent, B. (2000). Direct interaction of resistance gene and avirulence gene products confers rice blast resistance. EMBO J. **19:** 4004–4014.

Jiang, R.H.Y., Tripathy, S., Govers, F., and Tyler, B.M. (2008). RXLR effector reservoir in two Phytophthora species is dominated by a single rapidly evolving superfamily with more than 700 members. Proc. Natl. Acad. Sci. USA **105:** 4874–4879.

Kamoun, S. (2006). A catalogue of the effector secretome of plant pathogenic oomycetes. Annu. Rev. Phytopathol. **44:** 41–60.

Kamoun, S. (2007). Groovy times: Filamentous pathogen effectors revealed. Curr. Opin. Plant Biol. **10:** 358–365.

Kang, S., Sweigard, J.A., and Valent, B. (1995). The *PWL* host specificity gene family in the blast fungus *Magnaporthe grisea.* Mol. Plant Microbe Interact. **8:** 939–948.

Kankanala, P., Czymmek, K., and Valent, B. (2007). Roles for rice membrane dynamics and plasmodesmata during biotrophic invasion by the blast fungus. Plant Cell **19:** 706–724.

Kemen, E., Kemen, A.C., Rafiqi, M., Hempel, U., Mendgen, K., Hahn, M., and Voegele, R.T. (2005). Identification of a protein from rust fungi transferred from haustoria into infected plant cells. Mol. Plant Microbe Interact. **18:** 1130–1139.

Khang, C.H., Park, S., Rho, H., Lee, Y., and Kang, S. (2006). *Agrobacterium tumefaciens*-mediated transformation and mutagenesis of filamentous fungi *Magnaporthe grisea* and *Fusarium oxysporum*. In Agrobacterium Protocols, K. Wang, ed (Totowa, NJ: Humana Press), pp. 403–420.

Khang, C.H., Park, S.-Y., Lee, Y.-H., Valent, B., and Kang, S. (2008). Genome organization and evolution of the *AVR-Pita* avirulence gene family in the *Magnaporthe grisea* species complex. Mol. Plant Microbe Interact. **21:** 658–670.

Koga, H., Dohi, K., Nakayachi, O., and Mori, M. (2004). A novel inoculation method of *Magnaporthe grisea* for cytological observation of the infection process using intact leaf sheaths of rice plants. Physiol. Mol. Plant Pathol. **64:** 67–72.

Leung, H., Borromeo, E.S., Bernardo, M.A., and Notteghem, J.L.

(1988). Genetic analysis of virulence in the rice blast fungus *Magnaporthe grisea.* Phytopathology **78:** 1227–1233.

Li, W., et al. (2009). The *Magnaporthe oryzae* avirulence gene *AvrPiz-t* encodes a predicted secreted protein that triggers the immunity in rice mediated by the blast resistance gene *Piz-t.* Mol. Plant Microbe Interact. **22:** 411–420.

Mellersh, D.G., and Heath, M.C. (2001). Plasma membrane-cell wall adhesion is required for expression of plant defense responses during fungal penetration. Plant Cell **13:** 413–424.

Mendgen, K., and Hahn, M. (2002). Plant infection and the establishment of fungal biotrophy. Trends Plant Sci. **7:** 352–356.

Mims, C.W., and Richardson, E.A. (2007). Light and electron microscopic observations of the infection of *Camellia sasanqua* by the fungus *Exobasidum camelliae* var. *gracillis.* Can. J. Bot. **85:** 175–183.

Mims, C.W., Richardson, E.A., Holt III, B.F., and Dangl, J.L. (2004). Ultrastructure of the host-pathogen interface in *Arabidopsis thaliana* leaves infected by the downy mildew *Hyaloperonospora parasitica.* Can. J. Bot. **82:** 1001–1008.

Mosquera, G., Giraldo, M.C., Khang, C.H., Coughlan, S., and Valent, B. (2009). Interaction transcriptome analysis identifies *Magnaporthe oryzae* BAS1-4 as biotrophy-associated secreted proteins in rice blast disease. Plant Cell **21:** 1273–1290.

Mullins, E.D., Chen, X., Romaine, P., Raina, R., Geiser, D.M., and Kang, S. (2001). *Agrobacterium*-mediated transformation of *Fusarium oxysporum*: An efficient tool for insertional mutagenesis and gene transfer. Phytopathology **91:** 173–180.

Nelson, B.K., Cai, X., and Nebenführ, A. (2007). A multi-color set of in vivo organelle markers for colocalization studies in Arabidopsis and other plants. Plant J. **51:** 1126–1136.

O'Connell, R.J., and Panstruga, R. (2006). Tête à tête inside a plant cell: Establishing compatibility between plants and biotrophic fungi and oomycetes. New Phytol. **171:** 699–718.

Oparka, K.J., Roberts, A.G., Boevink, P., Santa Cruz, S., Roberts, I., Pradel, K.S., Imlau, A., Kotlizky, G., Sauer, N., and Epel, B. (1999). Simple, but not branched, plasmodesmata allow the nonspecific trafficking of proteins in developing tobacco leaves. Cell **97:** 743–754.

Orbach, M.J., Farrall, L., Sweigard, J.A., Chumley, F.G., and Valent, B. (2000). The fungal avirulence gene *AVR-Pita* determines efficacy for the rice blast resistance gene *Pi-ta.* Plant Cell **12:** 2019–2032.

Shaner, N.C., Lin, M.Z., McKeown, M.R., Steinbach, P.A., Hazelwood, K.L., Davidson, M.W., and Tsien, R.Y. (2008). Improving the photostability of bright monomeric orange and red fluorescent proteins. Nat. Methods **5:** 545–551.

Shinsuke, M., et al. (2009). Molecular cloning and characterization of the *AVR-Pia* locus from a Japanese field isolate of *Magnaporthe oryzae.* Mol. Plant Pathol. **10:** 361–374.

Shoji, J.-y., Arioka, M., and Kitamoto, K. (2008). Dissecting cellular components of the secretory pathway in filamentous fungi: Insights into their application for protein production. Biotechnol. Lett. **30:** 7–14.

Simon, U.K., Bauer, R., and Oberwinkler, F. (2004). The unique cellular interaction between the leaf pathogen *Cymadothea trifolii* and *Trifolium repens.* Mycologia **96:** 1209–1217.

Steinberg, G. (2007). Hyphal growth: A tale of motors, lipids, and the spitzenkoerper. Eukaryot. Cell **6:** 351–360.

Sweigard, J.A., Carroll, A.M., Kang, S., Farrall, L., Chumley, F.G., and Valent, B. (1995). Identification, cloning, and characterization of *PWL2*, a gene for host species specificity in the rice blast fungus. Plant Cell **7:** 1221–1233.

Sweigard, J.A., Chumley, F.G., and Valent, B. (1992). Cloning and analysis of *CUT1*, a cutinase gene from *Magnaporthe grisea.* Mol. Gen. Genet. **232:** 174–182.

Valent, B., Farrall, L., and Chumley, F.G. (1991). *Magnaporthe grisea* genes for pathogenicity and virulence identified through a series of backcrosses. Genetics **127:** 87–101.

Verma, D.P.S., and Hong, Z. (2005). The ins and outs in membrane dynamics: Tubulation and vesiculation. Trends Plant Sci. **10:** 159–165.

Veses, V., and Gow, N.A.R. (2009). Pseudohypha budding patterns of *Candida albicans.* Med. Mycol. **47:** 268–275.

Wang, G.-L., and Valent, B. (2009). Advances in Genetics, Genomics and Control of Rice Blast Disease. (New York: Springer Science and Business Media).

Whisson, S.C., et al. (2007). A translocation signal for delivery of oomycete effector proteins into host plant cells. Nature **450:** 115–118.

Wilson, R.A., and Talbot, N.J. (2009). Under pressure: Investigating the biology of plant infection by *Magnaporthe oryzae.* Nat. Rev. Microbiol. **7:** 185–195.

Yi, M., Chi, M.-H., Khang, C.H., Park, S.-Y., Kang, S., Valent, B., and Lee, Y.-H. (2009). The ER chaperone MoLHS1 is involved in asexual development and rice infection by the blast fungus *Magnaporthe oryzae.* Plant Cell **21:** 681–695.

Yoshida, K., Saitoh, H., Fujisawa, S., Kanzaki, H., Matsumura, H., Yoshida, K., Tosa, Y., Chuma, I., Takano, Y., Win, J., Kamoun, S., and Terauchi, R. (2009). Association genetics reveals three novel avirulence genes from the rice blast fungal pathogen *Magnaporthe oryzae.* Plant Cell **21:** 1573–1591.

Zambryski, P. (2004). Cell-to-cell transport of proteins and fluorescent tracers via plasmodesmata during plant development. J. Cell Biol. **164:** 165–168.

Zheng, H., Kunst, L., Hawes, C., and Moore, I. (2004). A GFP-based assay reveals a role for RHD3 in transport between the endoplasmic reticulum and Golgi apparatus. Plant J. **37:** 398–414.

Translocation of Magnaporthe oryzae Effectors into Rice Cells and Their Subsequent Cell-to-Cell Movement
Chang Hyun Khang, Romain Berruyer, Martha C. Giraldo, Prasanna Kankanala, Sook-Young Park, Kirk Czymmek, Seogchan Kang and Barbara Valent
PLANT CELL 2010;22;1388-1403; originally published online Apr 30, 2010;
DOI: 10.1105/tpc.109.069666

This information is current as of August 5, 2010

Supplemental Data	http://www.plantcell.org/cgi/content/full/tpc.109.069666/DC1
References	This article cites 59 articles, 16 of which you can access for free at: http://www.plantcell.org/cgi/content/full/22/4/1388#BIBL
Permissions	https://www.copyright.com/ccc/openurl.do?sid=pd_hw1532298X&issn=1532298X&WT.mc_id=pd_hw1532298X
eTOCs	Sign up for eTOCs for *THE PLANT CELL* at: http://www.plantcell.org/subscriptions/etoc.shtml
CiteTrack Alerts	Sign up for CiteTrack Alerts for *Plant Cell* at: http://www.plantcell.org/cgi/alerts/ctmain
Subscription Information	Subscription information for *The Plant Cell* and *Plant Physiology* is available at: http://www.aspb.org/publications/subscriptions.cfm

© American Society of Plant Biologists

ADVANCING THE SCIENCE OF PLANT BIOLOGY